AIAA JOURNAL
Vol. 38, No. 7, July 2000

Collision of a Vortex Jet with Stator Vanes

J. A. Lee* and A. T. Conlisk†
Ohio State University, Columbus, Ohio 43210-1107

We consider the unsteady behavior of the flowfield due to the slicing of a jet and a vortex with axial flow, that is, a vortex jet, by a pair of thin flat plates. In the case of a vortex, the geometry is an idealization of the collision between a tip vortex shed from a rotor blade and two downstream stator blades in an axial flow turbomachine. The flow is assumed to be inviscid, and the main result of the calculations is that the vorticity field near each plate is radically altered. The role of the axial flow in the vortex is to decrease the vortex core radius and to increase the swirl on the suction side while the vortex core radius increases and the swirl decreases on the pressure side. The suction peak due to the vortex grows on the suction side and decreases on the pressure side both for the jet and the vortex.

Nomenclature

a_v = vortex filament core radius, m
L = dimensionless computational boundary in the axial direction
p = dimensionless pressure
R = dimensionless computational boundary in the radial direction
r = dimensionless coordinate in the radial direction
r_v = radial coordinate of a point on a vortex filament, m
t = dimensionless time
t_w = timescale for wrapping of vorticity around the leading edge of the plate, s
U = speed of the plate, m/s
u = dimensionless velocity in the vortex in the radial direction
v = dimensionless velocity in the vortex in the azimuthal direction
v_I = dimensionless velocity in the vortex in the azimuthal direction at time t equals 0^-
W = average axial velocity in the vortex, m/s
w = dimensionless velocity in the vortex in the axial direction
w_I = dimensionless velocity in the vortex in the axial direction at time t equals 0^-
w_0 = maximum axial velocity in the vortex
z = dimensionless coordinate in the axial direction
Γ = dimensionless circulation
Γ^* = circulation, m^2/s
Δr = grid spacing in the radial direction
Δt = time step
Δz = grid spacing in the axial direction
θ = azimuthal coordinate
ξ = dimensionless axial component of vorticity
Ψ = dimensionless stream function
Ω = dimensionless circulation function, rv
ω = dimensionless azimuthal component of vorticity

I. Introduction

THE wake of rotating blades is complex, being three dimensional, in general, unsteady, and possessing considerable vorticity. The two main components of the wake of a rotating blade are the tip vortex shed as a result of the difference in velocity of the blade tip and the surrounding medium and an inboard trailing vortex sheet. In general the circulation around each blade is a maximum near the tip of the blade so that the tip vortex is stronger than the inboard sheet. Consequently, the tip vortex is of primary interest in these flows.

There are many situations where the wake of a rotating blade encounters a downstream body. This is the case when a helicopter rotor wake encounters the fuselage of the helicopter. Figure 1a shows an idealization of this situation. For simplicity only one blade is shown. The interaction region is noted, and the direction of the axial flow in the vortex is back toward the wing. We note that the vortex will eventually collide with the airframe first on the top and then as it convects down along the sides. This problem in helicopter aerodynamics has been addressed by a number of authors (Refs. 1–8, among many others). A related problem in helicopter aerodynamics is the blade–vortex interaction (BVI)[9–11] in which a tip vortex shed from a helicopter is sliced by a following blade. A list of current references to the BVI problem appear in several reviews.[12–14] Both of these problems fall within the class of helicopter flows referred to as interactional aerodynamics by Sheridan and Smith.[15] In addition, these interactions also occur in propeller flows and in axial flow turbomachines such as an axial flow blower, pump, or compressor, and a steam turbine. Sketches of these devices are given by Logan,[16] and a visualization of the tip vortex shed from a propeller is shown in Fig. 1a.[17]

We have termed a collision[18] an interaction in which a vortex is sliced by a plate in the sense that the core structure of the vortex, defined as a specified region of large vorticity surrounded by irrotational fluid, is substantially altered and even locally destroyed. The case of a jet or a vortex with axial flow, that is, a vortex jet, being sliced at a 90-deg angle by a single plate has been investigated by Lee et al.,[19,20] and this problem seems to reproduce many of the features of the full three-dimensional problem shown in Fig. 1. In the present paper, we consider the case where the jet or vortex is sliced by a pair of thin plates. This situation may occur when the tip vortex shed from a rotor blade collides with a pair of downstream stator vanes in an axial flow turbomachine. This situation is shown in Fig. 2a. Of course there is a large body of literature on the flow in various types of turbomachines, and there have been a number of studies on rotor–stator interaction.[21–27]

A complicating feature of these flows is that global numerical techniques are often inadequate because the local length scale, for example, the vortex core radius, is small and the timescale of any collision with a downstream surface is very short. Consider a portion of a tip vortex shed from an upstream rotor blade as shown in Fig. 2. Suppose we base the computational grid on the lengths $L_x = 0.05$ m; a hub radius of 0.152 m gives the azimuthal length $L_\theta = \pi \times 0.152\,\text{m} \sim 0.48\,\text{m}$, and we assume a stator vane length of $L_r = 0.152$ m. Suppose there are 200 points in each of the coordinate directions of the grid, r, θ, and x, surrounding the stator vanes, for a total of 8×10^6 grid points. A reasonable estimate of

Received 20 August 1998; revision received 7 October 1999; accepted for publication 17 November 1999.

*Graduate Research Assistant, Department of Mechanical Engineering; currently Senior Aeronautical Engineer, Cooper Turbo Compressor, Buffalo, NY 14225-0209.

†Professor, 206 W. 18th Avenue, Department of Mechanical Engineering. Associate Fellow AIAA.

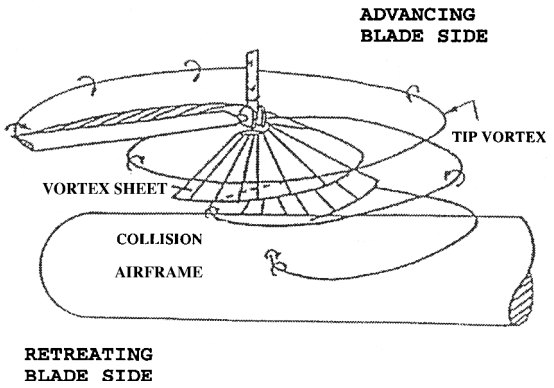

a)

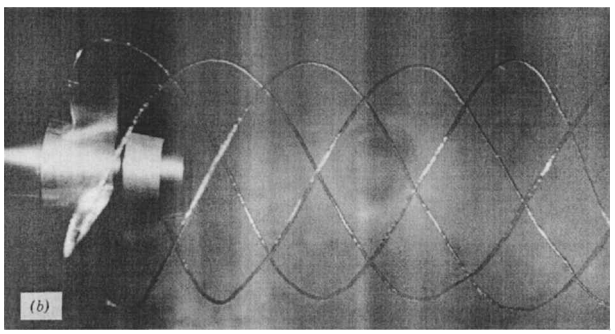

Fig. 1 Examples of possible tip-vortex and surface interaction: a) impingement of a tip vortex shed from a rotor blade on a cylindrical airframe[2] and b) tip vortex shed from a propeller; portions of the tip vortex may get sliced by downstream stator vanes if the propeller is ducted.

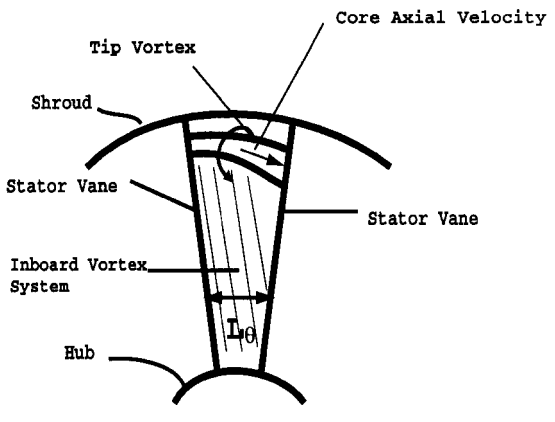

a) End View

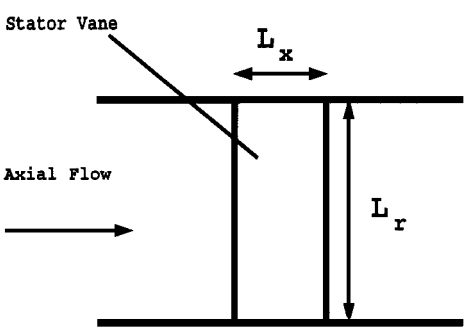

b) Side View

Fig. 2 Tip vortex and inboard sheet being sliced by two stator vanes; stator vanes have no twist.

the core of the vortex is about 1.27×10^{-3} m, which is approximately the width of typical rotor blades in this application. Then the nominal grid sizes are $R\Delta\theta \sim 2.39 \times 10^{-3}$ m, where R is the hub radius, $\Delta r \sim 7.6 \times 10^{-4}$ m, and $\Delta x = 2.54 \times 10^{-4}$ m. The most important directions are the x and r directions and in this scenario, the vortex would be represented by six points in the x direction and only one point in the radial direction. In addition, there are not enough points in the azimuthal direction to resolve the very rapid variation of the flow (even though the flow is assumed inviscid) near each stator vane. Because the three velocity components, the pressure, density and temperature, need to be computed, for the present case of 8×10^6 grid points, a minimum of 48 Mwords of memory are required for a single time step. Clearly this is a significant computational burden to resolve the flow on the scale of the vortex core. Thus, theoretical techniques combined with appropriately targeted numerical techniques are often required, and the calculations here resolve the vortex region directly.

In the calculations, we will neglect the influence of the boundary layer on the stator vanes in the calculations. We can show that, on the pressure side, this is reasonable, based on a dimensional analysis of the problem. Consider the case where there is a surrounding mean flow, for example, speed U_∞. Define the dimensionless circulation of a vortex as $\Gamma = \Gamma^* / U_\infty c = \mathcal{O}(1)$, where c is the chord of the stator vane, that is, L_x. Then the vortex Reynolds number, $Re_v = \Gamma^* / \nu$, is the same order of magnitude as the Reynolds number based on the stator vane length and the external mean velocity U_∞, that is, $Re = U_\infty c / \nu$. Here ν is the kinematic viscosity. Ting and Tung[28] have shown that the swirl velocity within the vortex is larger than the velocities in the neighboring fluid, that is, $\mathcal{O}(Re_v^{1/2})$, and so the flow in much of the vortex is inertially driven, and the flow may thus be assumed to be substantially inviscid in character. To see this, for $\Gamma = \Gamma^* / W_\infty c = \mathcal{O}(1)$, assume that the scaled vortex radius in laminar flow is $\mathcal{O}(Re^{-1/2})$, then from a simple Rankine vortex model the swirl velocity is $\mathcal{O}(Re^{1/2})$. Because the axial vorticity is essentially the radial derivative of the swirl, it is clear that the axial vorticity within the vortex core is of magnitude $\xi \sim Re$. Thus, the collision process may be considered inviscid until the swirl velocity is reduced to the order of magnitude of the surrounding boundary layer. What this means is that the Euler equations are sufficient to describe the process of vortex–vane collision, and indeed, these equations have been used to describe BVI in helicopter aerodynamics.[9]

The tip vortex shed from a rotor blade in a turbomachine can have a different character from the tip vortex shed from a helicopter rotor blade. This is because of the presence of the shroud and the character of the tip vortex varies widely with tip clearance.[29–31] When the tip vortex is strong and identifiable, it convects downstream and contracts inward away from the shroud based on continuity and momentum requirements. It will be helical in shape with the pitch of the helix dependent on the rotational speed of the rotor blade and the axial flow speed in the fan, among other parameters. The tip vortex will approach the downstream stator vanes and be sliced in the manner similar to the schematic of Fig. 2. This means that the swirl velocity in the core is reduced near each of the stator blades in a highly transient way.

We consider here a simplified model of the flow in Fig. 2, which is presented in Fig. 3. At time $t = 0$, a jet or vortex jet of specified structure is present in an undisturbed fluid. At time $t = 0^+$, a pair of flat plates are suddenly thrust at a right angle into the vortex so that the vortex is instantaneously and completely cut by the plate. This situation requires that the speed at which the plates is cut is much larger than the maximum velocity in the vortex. The objective is to determine the flow within the vortex for time $t > 0$. Because the axial velocity in the core of the vortex is unidirectional, the axial flow in the vortex will be toward one vane and away from the other. Thus, we have a pressure surface (axial velocity W toward the surface), as well as a suction surface (W away from the surface). In the results to follow, we show that the disturbance caused by the two bounding surfaces is everywhere finite on the timescale of the flow, which is given by a_v^2 / Γ^*, which is the smallest timescale of the problem. Note in this regard that rapid distortion theory,[32–35] which assumes a linearized disturbance on a much longer timescale, is often used to model flows in turbomachines with the objective of calculating the radiated acoustic field.

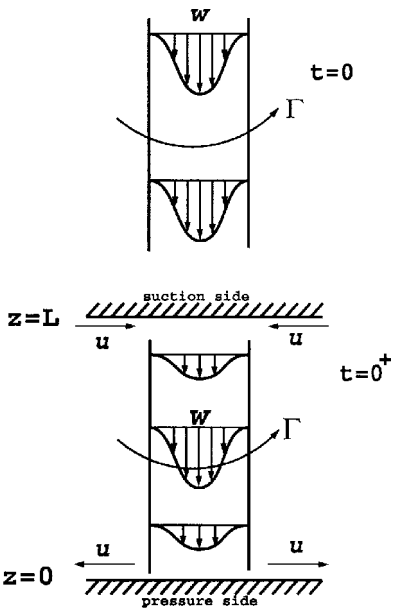

Fig. 3 Schematic of a vortex jet being sliced by a pair of blades.

We neglect the influence of compressibility in this paper and ignore the influence of the shroud. The results to be presented indicate a thinning of the vortex core at the suction surface along with a thickening of the vortex core at the pressure surface. Concurrent with this, the pressure on the suction surface is seen to focus, while the pressure suction peak at the pressure surface is reduced. This is consistent with the work of Lee et al.[20] for a single slicing surface.

II. Formulation

The governing equations are the axisymmetric Euler equations. All length scales are nondimensionalized by the initial vortex core radius a_v, whereas all velocities are nondimensionalized by the vortex jet velocity w_0. With an $*$ denoting the dimensional variables, the nondimensional variables are given as

$$t = t^* w_0 / a_v, \qquad r = r^* / a_v, \qquad z = z^* / a_v, \qquad \Gamma = \Gamma^* / w_0 a_v$$

$$u = u^* / w_0, \qquad v = v^* / w_0, \qquad w = w^* / w_0, \qquad \omega = \omega^* a_v / w_0$$

$$\Omega = \Omega^* / a_v w_0, \qquad \Psi = \Psi^* / w_0 a_v^2, \qquad p = p^* / \rho w_0^2 \tag{1}$$

Based on this nondimensionalization, the governing equations in cylindrical-polar coordinates (r, θ, and z), with velocity components $(u, v, w) = (v_r, v_\theta, v_z)$ are

$$\frac{\partial u}{\partial t} + u\frac{\partial u}{\partial r} + w\frac{\partial u}{\partial z} - \frac{v^2}{r} = -\frac{\partial p}{\partial r} \tag{2}$$

$$\frac{\partial v}{\partial t} + u\frac{\partial v}{\partial r} + w\frac{\partial v}{\partial z} + \frac{uv}{r} = 0 \tag{3}$$

$$\frac{\partial w}{\partial t} + u\frac{\partial w}{\partial r} + w\frac{\partial w}{\partial z} = -\frac{\partial p}{\partial z} \tag{4}$$

The continuity equation in cylindrical-polar coordinates for incompressible flow is given by

$$\frac{1}{r}\frac{\partial (ru)}{\partial r} + \frac{\partial w}{\partial z} = 0 \tag{5}$$

The numerical domain of solution is now $0 \le r \le R$, where $R = R^*/a_v$ and $0 \le z \le L$, where $L = L^*/a_v$. The azimuthal and axial components of vorticity are defined by

$$\omega = \frac{\partial u}{\partial z} - \frac{\partial w}{\partial r}, \qquad \xi = \frac{1}{r}\frac{\partial}{\partial r}(rv) \tag{6}$$

There is a radial component of the vorticity, but it is not required in this formulation.

To solve these equations, we replace the velocity components u, v, and w with the vorticity ω and the stream function Ψ. Equation (5) is satisfied by the existence of a stream function Ψ, which is defined by the radial and axial velocity components as

$$u = -\frac{1}{r}\frac{\partial \Psi}{\partial z} \tag{7}$$

$$w = \frac{1}{r}\frac{\partial \Psi}{\partial r} \tag{8}$$

and Eq. (6) yields

$$\omega = -\frac{\partial}{\partial z}\left(\frac{1}{r}\frac{\partial \Psi}{\partial z}\right) - \frac{\partial}{\partial r}\left(\frac{1}{r}\frac{\partial \Psi}{\partial r}\right) = -\frac{1}{r}D^2\Psi \tag{9}$$

and Eq. (3) for the circulation function ($\Omega = rv$) becomes

$$\frac{\partial \Omega}{\partial t} + u\frac{\partial \Omega}{\partial r} + w\frac{\partial \Omega}{\partial z} = 0 \tag{10}$$

The inviscid, axisymmetric azimuthal vorticity transport equation is found by combining the momentum equations (2) and (4) and is given by

$$\frac{\partial \omega}{\partial t} + u\frac{\partial \omega}{\partial r} + w\frac{\partial \omega}{\partial z} - \frac{u\omega}{r} - 2\frac{v}{r}\frac{\partial v}{\partial z} = 0 \tag{11}$$

with u and w given by Eqs. (7) and (8). Equations (9–11) are solved simultaneously for the three unknowns Ψ, $v = \Omega/r$, and ω.

Four boundary conditions are needed for the elliptic equation (9). For time $t > 0$, the axial velocity w must be zero on the walls and, hence,

$$\Psi = 0 \qquad \text{on} \qquad z = 0 \tag{12}$$

$$\Psi = 0 \qquad \text{on} \qquad z = L \tag{13}$$

Similarly, on $r = 0$, u must be zero, yielding

$$\Psi = 0 \qquad \text{on} \qquad r = 0 \tag{14}$$

The axial velocity vanishes as $r \to \infty$ and so

$$\frac{\partial \Psi}{\partial r} = 0 \qquad \text{on} \qquad r = R \tag{15}$$

provided R is sufficiently large.

The hyperbolic equations (10) and (11) also require spatial initial conditions specified on the inflow boundary $z = L$ for the case where the initial axial velocity is from the top wall to the bottom wall. Given the velocities from the solution of the stream function, the hyperbolic equations are swept from $z = L$ to 0; because of the coupling between the three equations, iteration is employed, as will be discussed next.

The pressure is obtained by integrating Eqs. (2) and (4) with the reference pressure taken at $r = R$, $z = 0$. That is, Eq. (4) is solved on $r = R$, with the reference pressure being $p(R, 0, 0) = 0$. Equation (2) is used to solve for the pressure elsewhere, with the reference pressure being $p(R, z, t)$. For example, if Eq. (4) is expressed in conservative form, then the pressure on $r = R$ is given by

$$p(R, z, t) = -\int_0^z \left(\frac{\partial w}{\partial t} + \frac{1}{r}\frac{\partial}{\partial r}(ruw) + \frac{\partial}{\partial z}(w^2)\right)dz \tag{16}$$

and integrating Eq. (2) similarly yields

$$p(r, z, t) = \int_r^R \left(\frac{\partial u}{\partial t} + \frac{1}{r}\frac{\partial}{\partial r}(ru^2) + \frac{\partial}{\partial z}(uw) - \frac{v^2}{r}\right)dr + p(R, z, 0) \tag{17}$$

where we have assumed that R is large enough so that $p(R, z, t) = p(R, z, 0)$.

The initial conditions correspond to an undisturbed vortex with axial flow. In this regard, it is expected that the response to the instantaneous presence of the wall will have characteristics of both

a jet and a vortex. Thus, the term vortex jet is used by Lee et al.[20] The initial axial velocity distribution for this flow is

$$w = w_I = -e^{-r^2} \tag{18}$$

where the negative sign denotes that the axial velocity is downward toward the bottom wall. The initial radial velocity vanishes.

The initial swirl velocity distribution is taken to be a Lamb-type vortex (see Ref. 24):

$$v = v_I = (\Gamma/2\pi r)\left(1 - e^{-r^2}\right) \tag{19}$$

corresponding to a decayed potential vortex with a linear swirl as $r \to 0$. The initial circulation distribution is then

$$\Omega = \Omega_I = rv_I = (\Gamma/2\pi)\left(1 - e^{-r^2}\right) \tag{20}$$

leading to

$$\xi_I = \frac{1}{r}\frac{\partial v}{\partial r} = \frac{\Gamma}{\pi}e^{-r^2} \tag{21}$$

Note that the initial axial vorticity is a maximum at $r = 0$ and decays to zero as $r \to \infty$.

The numerical solution to Eq. (9) subject to boundary conditions (12–15) is calculated using a standard finite difference scheme, and this is described by Lee et al.[20] The pressure is obtained by numerical integration of Eqs. (16) and (17) using a second-order-accurate trapezoidal rule. The unsteady terms are calculated using a three-point second-order backward difference in time. A multigrid scheme was employed to accelerate convergence. Additional details are given by Lee et al.[20]

Numerical solutions have been computed for three sets of grids corresponding to $(64)^2$, $(128)^2$, and $(256)^2$ points, for $R = L = 4$, and the results for the velocities and the vorticity for each grid were compared. It was found that at least two-figure spatial accuracy is achieved using 128 grid points in both r and z. At least two-digit accuracy in all variables is achieved using a time step of $\Delta t = 0.01$, when compared with solutions for $\Delta t = 0.005$; three-digit accuracy is obtained over the vast majority of grid points. In addition, the effects of the lengths of the computational domain in r and z on the numerical solution for the case of no swirl was tested, resulting in a 2.9% change in the azimuthal vorticity on the wall when R and L are doubled from 4 to 8. Because it is a derived quantity based on a derivative of the velocity field, the test on the azimuthal vorticity is more stringent than a test on other quantities such as velocity and even pressure inasmuch as the pressure is obtained from an integration. The grid spacing was held fixed at $\Delta r = \Delta z = 0.0312$, with $\Delta t = 0.01$, and the convergence criterion $\epsilon = 10^{-7}$ for these tests. All of the results presented here are for 128 points in both directions with $R = L = 4$, $\Delta t = 0.01$.

III. Results

We have assumed that the vortex is instantaneously sliced; in reality we would expect a thin layer of vorticity to be wrapped around the leading edge of each vane. The timescale associated with the wrapping of vorticity around the leading edge is $t_w \sim a_v/U$, where a_v is the vortex core radius and U is the speed of the plate. The timescale associated with the axial flow is $t_W \sim a_v/W$, where W is the axial velocity scale. For the dimensionless circulation $\Gamma = \mathcal{O}(1)$, this timescale is of the same order of magnitude as the vortex timescale $t_v \sim a_v^2/\Gamma^*$. If the axial flow timescale and the timescale associated with the wrapping are sufficiently different, then these two phenomena will not interact. Thus, if $U \gg W$, then the timescale of the wrapping is much shorter than the redistribution process. Moreover, the axial vortex lines are reoriented by the plate so that they lie in the radial direction, and the portions on the top and bottom of the plate cancel each other because those portions have opposite-signed vorticity.

A. Pure Jet

We first consider the case of a pure jet with no swirl to establish the fundamental features of the flow. Figure 4 shows the azimuthal vorticity on the walls. The initial condition is indicated by $*$, with

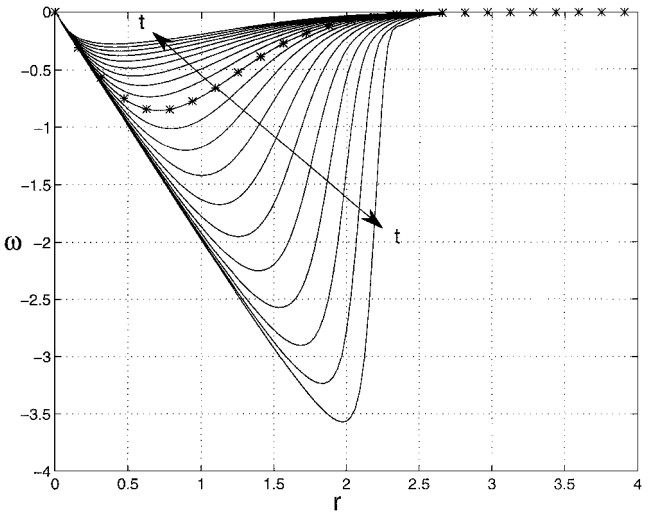

Fig. 4 Azimuthal vorticity on the suction side (top arrow) and pressure side (bottom arrow) for the pure jet.

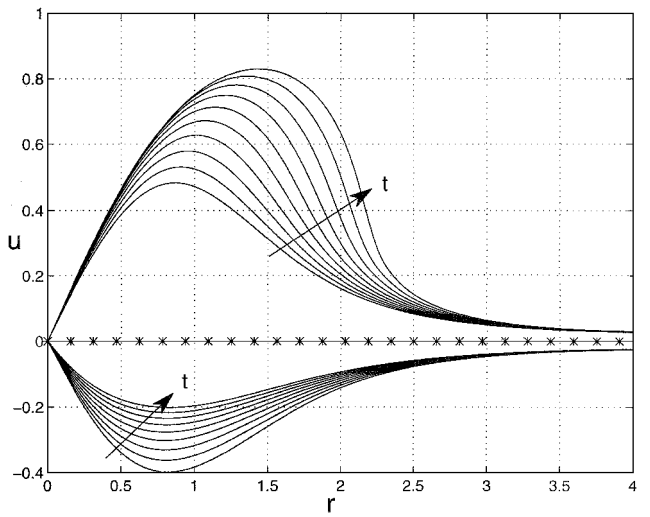

Fig. 5 Radial velocity on the suction side (bottom arrow) and pressure side (top arrow) for the pure jet.

arrows in the direction of increasing time. Every 25th time step is plotted until $t = 2.5$. From the definition of the vorticity vector, the azimuthal vorticity is associated with the presence of axial flow. Note how the azimuthal vorticity on the suction side decreases substantially, while on the pressure side, the azimuthal vorticity continually increases. The pressure side behavior is supported by an analytical solution for the single-wall case as discussed by Lee et al.[20] Indeed these results are similar to those for the single-wall cases described by Lee et al.[20] The reduction in azimuthal vorticity on the suction side is due to the convection of azimuthal vorticity away from the suction side by the axial velocity. Hence, the azimuthal vorticity is being redistributed from the suction side to the pressure side.

Figure 5 shows the radial velocity on the suction and pressure sides for the times as in Fig. 4. The initial condition $(*)$ is $u = 0$ at $t = 0$, and arrows are in the direction of increasing time. Here the radial velocity on the pressure side decreases in magnitude with time, as a result of flow being convected away from the suction side. On the pressure side, the radial velocity steadily grows.

Figure 6 shows the pressure on the suction side and pressure side for the case of no swirl for the same times as in Fig. 4. The initial condition is $p = 0$ at $t = 0$, and arrows are in the direction of increasing time. It can be seen that on the suction side the pressure decreases as time increases, corresponding to the decrease in the azimuthal vorticity in the region near the suction side. On the pressure side, the pressure grows near the axis $r = 0$ and then begins

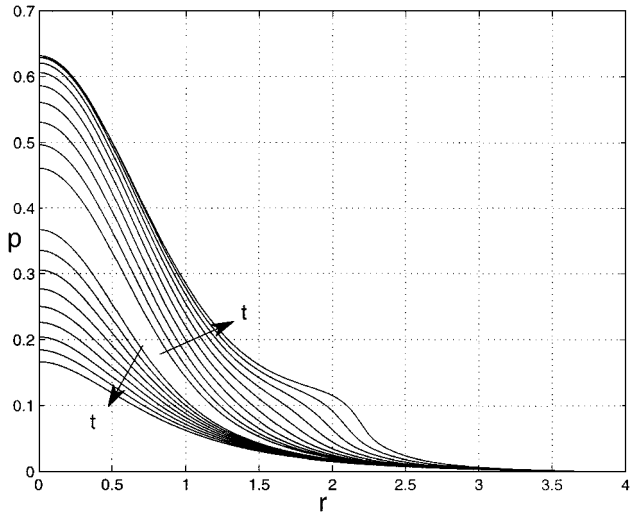

Fig. 6 Pressure on the suction side (bottom arrow) and pressure side (top arrow) for the pure jet.

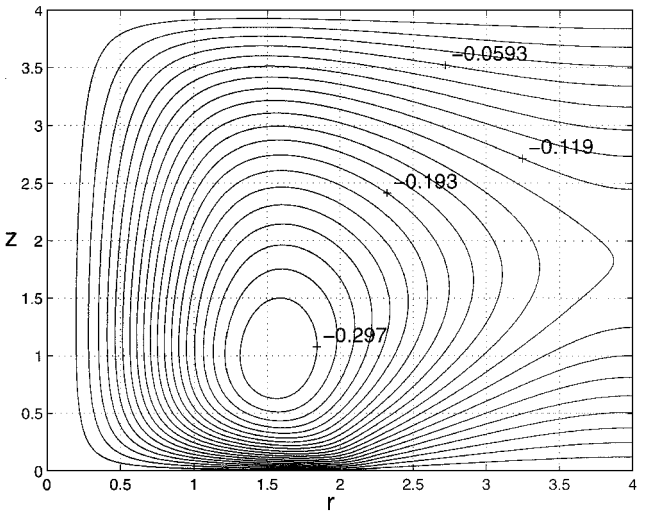

Fig. 7 Streamlines for the pure jet at time $t = 2.5$.

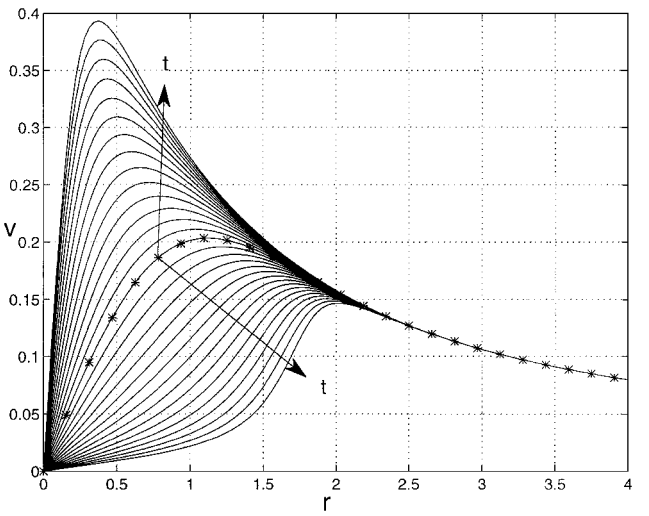

Fig. 8 Swirl velocity on the suction side surface (top arrow) and pressure side surface (bottom arrow) for the vortex jet for $\Gamma = 2.0$.

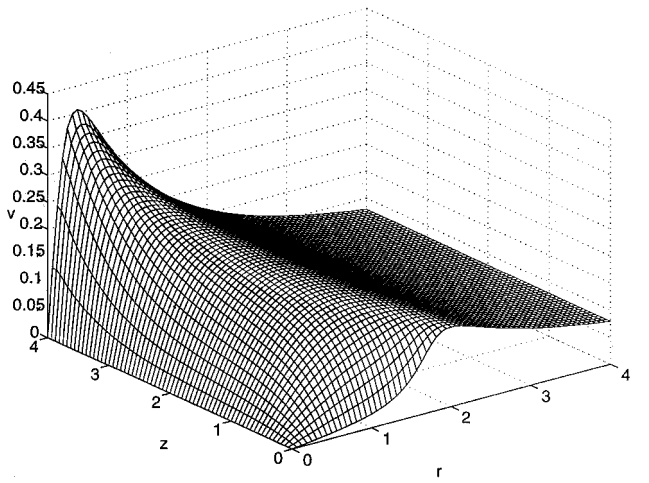

Fig. 9 Three-dimensional plot of the swirl velocity for the vortex jet for $\Gamma = 2.0$ at $t = 1.5$; note that the disturbance caused by the wall is everywhere finite on this timescale.

to relax at about $t = 2.5$ due to the decrease in radial velocity. In fact, the pressure in the entire domain is expected to approach zero because there is no steady inflow of fluid. The only inflow of fluid comes from the radial inflow on the suction side, and that is only in response to the stagnation in axial velocity in that region. Hence, in this inviscid problem, the steady solution is expected to be a region of stagnant fluid.

If the vortex core radius is about 1.3×10^{-3} m and the maximum axial velocity in the core is 30 m/s, then the total dimensional time is about 10^{-4} s. This time will be less than the time it takes for the vortex to pass the trailing edge of a stator vane having a chord 0.05 m and traveling at a velocity greater than about 100 m/s.

The streamlines at time $t = 2.5$ are shown in Fig. 7. Fluid is traveling in from the upper right-hand corner of Fig. 7 and exiting from the lower right-hand corner. By this time, the streamlines have clustered near the pressure side, in the region of high azimuthal vorticity. Note that $z = 0$ is the pressure side and that $z = 4$ is the suction side.

The driving force of the flow in this case is the azimuthal vorticity. The azimuthal vorticity is convected toward the pressure side by the axial velocity, resulting in a stagnant region of fluid extending from the suction side growing in time toward the pressure side. This dead region of fluid results from the cutting off of the jet at $z = L$, and, hence, there is no supply of azimuthal vorticity into the flow. Even though there is a radial inflow of fluid at the suction side, that fluid is irrotational. The main features of this flow are the region of growing azimuthal vorticity near the pressure side and the region of decreasing azimuthal vorticity near the suction side.

Having established the features of the flow without swirl, we now examine the case with swirl.

B. Vortex-Jet

We investigate the results for the dimensionless circulation $\Gamma = 2$. The swirl velocity is shown in Fig. 8 for the suction side (top arrow) and pressure side (bottom arrow). As in the preceding section, the initial condition is indicated by $*$, and arrows are in the direction of increasing time. In all figures in this section, where applicable, every 10th time step is plotted until $t = 1.5$. It can be seen that the swirl velocity focuses on the suction side and spreads radially outward on the pressure side. On the suction side, the focusing is in response to a radial inflow of fluid as a result of the stagnation of the jet on the suction side. On the pressure side, the resulting spreading of swirl is due to a radial outflow of fluid. Both of these phenomena occur in the single wall cases[20] and are central features of the collision process.

The influence of the two surfaces is significant in the sense that the disturbance extends a significant distance into the region between the two walls. In Fig. 9 is a three-dimensional plot of the swirl velocity. Note the focusing near the suction wall and the spreading along the pressure wall as shown in Fig. 8 at the wall. Also, from Fig. 8, it is seen that the disturbance caused by the two walls on this timescale is everywhere a finite disturbance. Clearly, the swirl velocity cannot continue to focus on the suction side, and this is one area in which viscosity will play a significant role. The phenomenon of viscous limiting of vortex core thinning is suggested in the study

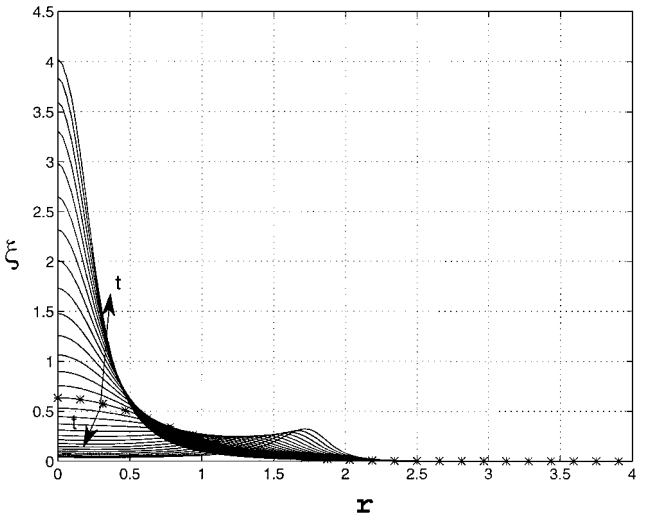

Fig. 10 Axial vorticity on the suction side (top arrow) and pressure side (bottom arrow) for the vortex jet with $\Gamma = 2.0$.

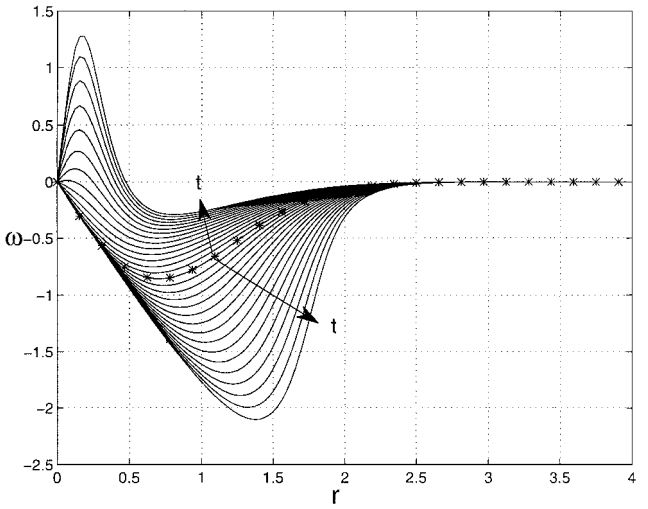

Fig. 11 Azimuthal vorticity on the suction side (top arrow) and pressure side (bottom arrow) for the vortex jet for $\Gamma = 2.0$.

by Burggraf et al.,[32] who show that boundary-layer fluid is drawn into a vortex oriented normal to a wall. This will halt the focusing of the swirl velocity. It should be noted in this regard that rapid distortion theory,[33–36] which assumes a linearized disturbance on a much longer timescale, is often used to model turbomachinery flows with the objective of calculating the radiated acoustic field.

Figure 10 shows the axial vorticity on the suction side surface (top arrow) and pressure side (bottom arrow). The suction side shows an increase in axial vorticity, which corresponds to a focusing of the vortex locally on the suction side. On the pressure side, the axial vorticity decreases as the vortex bulges radially outward.

Figures 8–10 illustrate the vortex properties of the vortex jet. The azimuthal vorticity that is associated with the jet properties of the flow is shown in Fig. 11. On the suction side, the azimuthal vorticity reduces in magnitude with time, and the waves are convected radially inward by the radial velocity. The reduction in azimuthal vorticity on the suction side is due to the convection of azimuthal vorticity away from the suction side by the axial velocity. It can be seen here that the addition of swirl causes the azimuthal vorticity on the suction side to change sign, causing a secondary flow near $r = 0$. The effect of swirl on the pressure side is to reduce the magnitude of azimuthal vorticity that would normally occur in a no-swirl flow.

Figure 12 shows the pressure on the pressure side (top arrow) and the suction side (bottom arrow). On the pressure side it can be seen that the pressure increases with time. Note that the outward traveling wave, which exists in the no-swirl flow, does not occur here. On the suction side, the pressure focuses with time, a swirl-dominated effect.

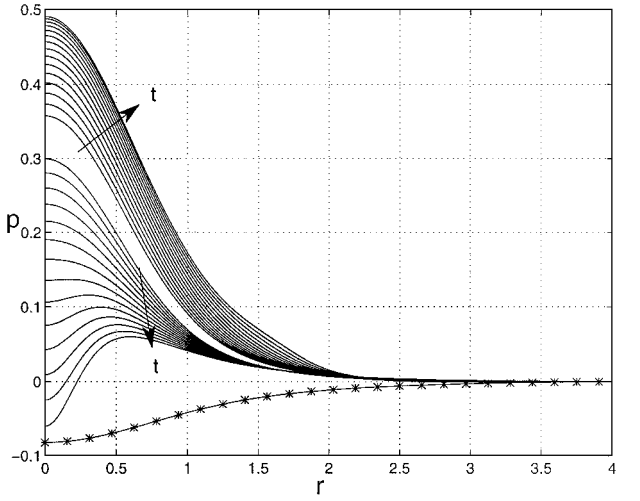

Fig. 12 Pressure on the suction side (bottom arrow) and pressure side (top arrow) for the vortex jet for $\Gamma = 2.0$.

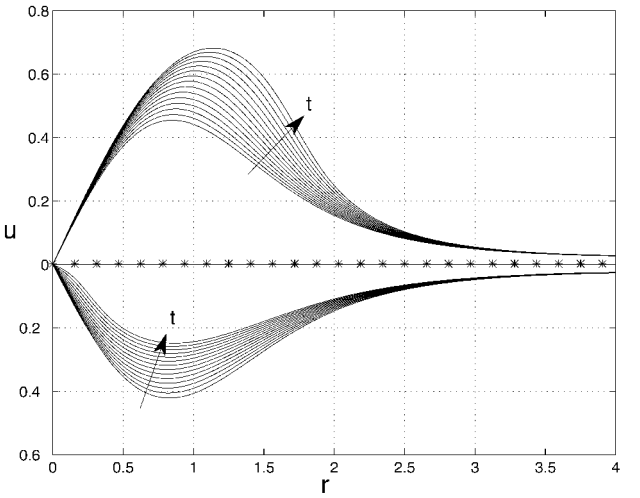

Fig. 13 Radial velocity on the suction side (bottom arrow) and pressure side (top arrow) for the vortex jet for $\Gamma = 2.0$.

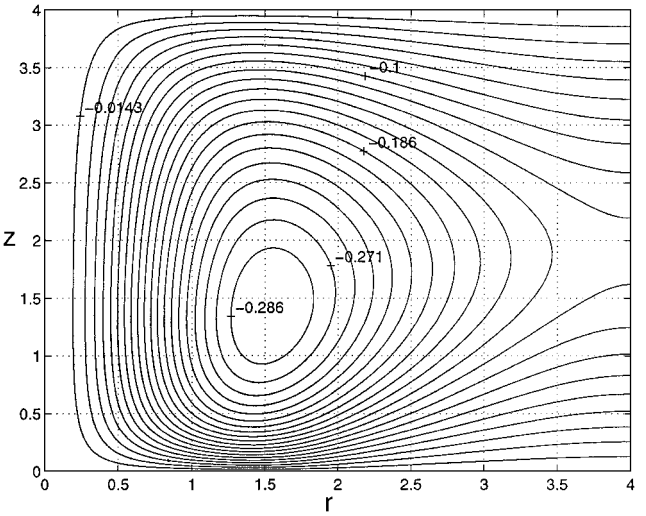

Fig. 14 Streamlines for $\Gamma = 2.0$ at time $t = 1.5$.

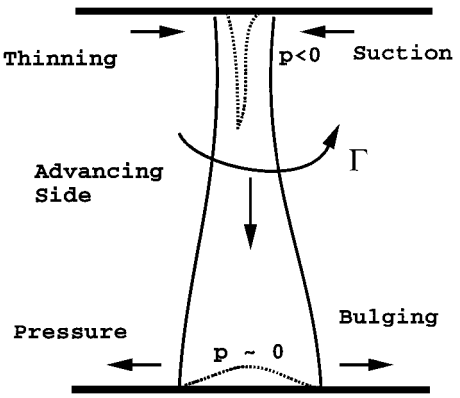

Fig. 15 Summary of the collision indicating the bulging on the pressure side and thinning on the suction side; behavior of the pressure under the vortex on each side is also shown.

The radial velocity profiles are shown in Fig. 13 for the pressure side (top arrow) and the suction side (bottom arrow). It can be seen here that the addition of swirl causes the radial velocity on the wall to be smaller in magnitude than in the no-swirl case. On the pressure side, the radial velocity increases with time, and on the suction side, the radial velocity decreases due to the redistribution of vorticity from the suction side to the pressure side. Figure 14 shows the streamlines at time $t = 1.5$. Fluid is moving in the same direction as in the pure jet case and is remarkably similar to that shown in Fig. 7 with flow from the upper right-hand corner to the lower right-hand corner, as for the pure jet. Note that $z = 0$ is the pressure side, and $z = 4$ is the suction side.

The problem described can be viewed as a simplified model for the collision of a tip vortex with a pair of stator vanes in an axial flow turbomachine. The physical phenomena described may also occur in centrifugal designs as well; indeed, Arndt et al.[26] indicate that unsteady pressures are much larger in magnitude on the suction side of the stator vane and those on the pressure side are much lower. This is precisely what is indicated in the present computations. Of course, the problem is much more complicated that the simplified problem discussed here. We have not considered the influence of compressibility, although this should not have a great impact on the qualitative aspects of the flow unless the flow is locally transonic. We have not considered the influence of the shroud, a mean flow, or turbulence. These issues will likely alter the details of the collision but not the basic conclusions. It is useful to sketch the flow behavior in qualitative terms and this is shown in Fig. 15. The suction peak grows on the wall where the axial velocity is away from the wall; on the other hand, the suction peak is removed and $p \sim 0$ when the axial velocity is toward the wall.

IV. Summary

We have calculated solutions for the collision of a vortex with two fixed surfaces oriented at right angles to the vortex. For the jet, the azimuthal vorticity is convected outward with the induced radial velocity on the pressure side. On the suction side, the azimuthal vorticity is greatly decreased. For the vortex jet, the azimuthal vorticity is similar to that of the pure jet on the pressure side; however, on the suction side, a relatively large positive value of the azimuthal vorticity is seen near $r = 0$. The axial vorticity in the core of the vortex jet is reduced significantly on the pressure side by $t = 1.5$. This reduction is evidenced by the reduction of the suction peak. On the suction side, the swirl velocity focuses, as does the pressure, and hence, the vortex persists. The primary effect of the presence of the two plates is to inviscidly redistribute the vorticity field.

We have neglected the influence of viscosity on the collision process and have shown that this is reasonable using dimensional analysis. During the collision process, where the axial flow in the vortex is directed toward the surface, the magnitude of the vorticity field within the vortex will be reduced to the order of magnitude of the boundary-layer vorticity, in which case distinguishing between boundary layer and vortex vorticity becomes impossible. The essence of the vorticity redistribution process is that vorticity is not destroyed but merely redistributed in an inviscid way. Coinciding with this redistribution of vorticity is the reduction of the suction peak associated with the original vortex. Of course, viscosity must become important in the region where the swirl velocity is low, and this occurs in what was once the core of the vortex. The same arguments apply to the pure jet if the axial velocity in the jet is much greater than the mean streaming motion. The axial velocity may be related to the tip speed of the rotating stage. Viscous effects will also be important in the region where the core axial velocity is away from the wall, as discussed in the preceding section.

References

[1]Affes, H., and Conlisk, A. T., "A Model for Rotor Tip Vortex–Airframe Interaction, Part 1: Theory," *AIAA Journal*, Vol. 31, No. 12, 1993, pp. 2263–2273.

[2]Affes, H., Conlisk, A. T., Kim, J. M., and Komerath, N. M., "A Model for Rotor Tip Vortex–Airframe Interaction, Part 2: Comparison with Experiment," *AIAA Journal*, Vol. 31, No. 12, 1993, pp. 2274–2282.

[3]Kim, J. M., and Komerath, N. M., "Summary of the Interaction of a Rotor Wake with a Circular Cylinder," *AIAA Journal*, Vol. 33, No. 3, 1995, pp. 470–478.

[4]Liou, S. G., Komerath, N. M., and McMahon, N. M., "Measurement of the Interaction Between a Rotor Tip Vortex and a Cylinder," *AIAA Journal*, Vol. 28, No. 6, 1990, pp. 975–981.

[5]Radcliff, T. D., Burggraf, O. R., and Conlisk, A. T., "Axial Core Flow Effects on the Interaction of a Rotor-Tip Vortex with an Airframe," AIAA Paper 97-0658, Jan. 1997.

[6]Mahalingam, R., Komerath, N. M., Radcliff, T. D., Burggraf, O. R., and Conlisk, A. T., "Vortex-Surface Collision: 3-Dimensional Core Flow," AIAA Paper 97-2061, June 1997.

[7]Brand, A. G., McMahon, H. M., and Komerath, N. M., "Correlations of Rotor Wake Airframe Interaction Measurements and Flow Visualization Data," *Journal of the American Helicopter Society*, Vol. 35, No. 4, 1990, pp. 4–15.

[8]Leishman, J. G., and Bi, N., "Aerodynamic Interactions Between a Rotor and a Fuselage in Forward Flight," *Journal of the American Helicopter Society*, Vol. 35, No. 3, 1990, pp. 22–31.

[9]Hassan, A. A., Tung, C., and Sankar, L. N., "Euler Solutions for Self-Generated Rotor Blade-Vortex Interactions," *International Journal for Numerical Methods in Fluids*, Vol. 15, No. 4, 1992, pp. 427–451.

[10]Tung, C., Yu, Y. H., and Low, S. L., "Aerodynamic Aspects of BVI," AIAA Paper 96-2010, June 1996.

[11]Marshall, J. S., "Vortex Cutting by a Blade, Part I: General Theory and a Simple Solution," *AIAA Journal*, Vol. 32, No. 6, 1994, pp. 1145–1150.

[12]McCroskey, W. J., "Vortex Wakes of Rotorcraft," AIAA Paper 95-0530, Jan. 1995.

[13]Conlisk, A. T., "Modern Helicopter Aerodynamics," *Annual Review of Fluid Mechanics*, Vol. 27, 1997, pp. 515–567.

[14]Yu, Y. H., "Rotor Blade-Vortex Interaction Noise: Generating Mechanisms and Control Concepts," *Proceedings of the AHS 2nd International Aeromechanics Specialists' Conference*, Vol. 1, 1995, pp. 3.1–3.12.

[15]Sheridan, P. F., and Smith, R. F., "Interactional Aerodynamics—A New Challenge to Helicopter Technology," *Journal of the American Helicopter Society*, Vol. 25, No. 1, 1980, pp. 3–21.

[16]Logan, E., Jr., *Turbomachinery: Basic Theory and Applications*, Marcel Dekker, New York, 1981, Chap. 1.

[17]Arndt, R. E. A., "Cavitation in Fluid Machinery and Hydraulic Structures," *Annual Review of Fluid Mechanics*, Vol. 13, 1981, pp. 273–328.

[18]Conlisk, A. T., "A Theory of Vortex-Surface Collisions," AIAA Paper 98-2858, June 1998.

[19]Lee, J., Xiao, Z., Burggraf, O. R., Conlisk, A. T., and Komerath, N. M., "An Inviscid Approach to Vortex-Surface Collisions," AIAA Paper 95-2237, June 1995.

[20]Lee, J. A., Burggraf, O. R., and Conlisk, A. T., "On the Impulsive Blocking of a Vortex-Jet," *Journal of Fluid Mechanics*, Vol. 369, Sept. 1998, pp. 301–331.

[21]Dawes, W. N., "A Simulation of the Unsteady Interaction of a Centrifugal Impeller with Its Vaned Diffuser: Flow Analysis," *Journal of Turbomachinery*, Vol. 117, No. 2, 1995, pp. 213–222.

[22]Dring, R. P., Joslyn, H. D., Hardin, L. W., and Wagner, J. H., "Turbine Rotor–Stator Interaction," *Journal of Engineering for Power*, Vol. 104, No. 4, 1982, pp. 729–742.

[23]Valkov, T., and Tan, C. S., "Control of the Unsteady Flow in a Stator Blade Row Interacting with Upstream Moving Wakes," *Journal of Turbomachinery*, Vol. 117, No. 2, 1995, pp. 97–105.

[24]Saxer, A. P., and Giles, M. B., "Predictions of Three-Dimensional Steady and Unsteady Inviscid Transonic Stator/Rotor Interaction with Inlet Radial Temperature Nonuniformity," *Journal of Turbomachinery*, Vol. 116, No. 3, 1994, pp. 347–357.

[25] Smith, L. H., "NASA/GE Fan and Compressor Research Accomplishments," *Journal of Turbomachinery*, Vol. 116, No. 4, 1994, pp. 555–569.

[26] Arndt, N., Acosta, A. J., Brennen, C. E., and Caughey, T. K., "Rotor–Stator Interaction in a Diffuser Pump," *Journal of Turbomachinery*, Vol. 111, No. 3, 1989, pp. 213–221.

[27] Fleeter, S., Jay, R. L., and Bennett, W. A., "Time Variant Aerodynamic Response of a Stator Row Including the Effects of Airfoil Camber," *Journal of Engineering for Power*, Vol. 102, No. 2, 1980, pp. 334–343.

[28] Ting, L., and Tung, C., "Motion and Decay of a Vortex in a Nonuniform Stream," *Physics of Fluids*, Vol. 8, No. 6, 1965, pp. 1039–1051.

[29] Groeneweg, J. F., "Noise Sources," *Aeroacoustics of Flight Vehicles: Theory and Practice*, NASA Reference Publ. 1258, Vol. 1, Aug. 1991.

[30] Qin, W., and Tsukamoto, H., "Theoretical Study of Pressure Fluctuations Downstream of a Diffuser Pump Impeller—Part 2: Effects of Volute, Flow Rate and Radial Gap," *Journal of Fluids Engineering*, Vol. 119, Sept. 1997, pp. 653–658.

[31] Laksminarayana, B., Zaccaria, M., and Marathe, B., "The Structure of Tip-Clearance Flow in Axial Flow Compressors," *Journal of Turbomachinery*, Vol. 117, July 1995, pp. 336–347.

[32] Burggraf, O. R., Stewartson, K., and Belcher, R., "Boundary Layer Induced by a Potential Vortex," *Physics of Fluids*, Vol. 14, No. 9, 1971, pp. 1821–1833.

[33] Savill, A. M., "Recent Developments in Rapid-Distortion Theory," *Annual Review of Fluid Mechanics*, Vol. 19, 1987, pp. 531–575.

[34] Atassi, H. M., "Unsteady Aerodynamics of Vortical Flows: Early and Recent Developments," *Aerodynamics and Aeroacoustics IV*, edited by K.-Y. Fung, World Scientific, Singapore, 1994, pp. 121–172.

[35] Groeneweg, J. F., Sofrin, T. G., Gliebe, P. R., and Rice, E. J., "Turbomachinery Noise," *Aeroacoustics of Flight Vehicles: Theory and Practice, Volume 1: Noise Sources*, edited by H. H. Hubbard, NASA RP-1258, Vol. 1, WRDC TR 90-3052, Aug. 1991, Chap. 1.

[36] Envia, E., Huff, D. L., and Morrison, C. R., "Analytical Assessment of Stator Sweep and Lean in Reducing Rotor-Stator Noise," AIAA Paper 96-1791, 1996.

J. C. Hermanson
Associate Editor